

## Electronic Supplementary Information

### Origin of electrocatalytic nitrogen reduction activity over transition metal disulfides: critical role of *in situ* generation of S vacancy

Tianyi Wang<sup>1</sup>, Zhongyuan Guo<sup>2</sup>, Hirofumi Oka<sup>1</sup>, Akichika Kumatani<sup>1,3,4,5,\*</sup>, Chuangwei Liu<sup>6,\*</sup>, and Hao Li<sup>1,\*</sup>

<sup>1</sup> Advanced Institute for Materials Research (WPI-AIMR), Tohoku University, Sendai, 980-8577, Japan

<sup>2</sup> College of Environmental and Resource Sciences, Zhejiang University, Hangzhou, 310058, China

<sup>3</sup> Institute of Engineering Innovation (IEI), School of Engineering, The University of Tokyo, Tokyo, 113-8656, Japan

<sup>4</sup> Precursory Research for Embryonic Science and Technology (PRESTO), Japan Science and Technology Agency (JST), Saitama 332-0012, Japan

<sup>5</sup> Graduate School of Environmental Studies & Center for Science and Innovation in Spintronics (CSIS), Tohoku University, Sendai, Miyagi 980-8579, Japan

<sup>6</sup> Key Lab for Anisotropy and Texture of Materials School of Materials Science and Engineering, Northeastern University, Shenyang, 110819, China

#### \* Corresponding Authors

Email: [kumatani@g.ecc.u-tokyo.ac.jp](mailto:kumatani@g.ecc.u-tokyo.ac.jp) (A. K.)

Email: [liucw@mail.neu.edu.cn](mailto:liucw@mail.neu.edu.cn) (C. L.)

Email: [li.hao.b8@tohoku.ac.jp](mailto:li.hao.b8@tohoku.ac.jp) (H. L.)

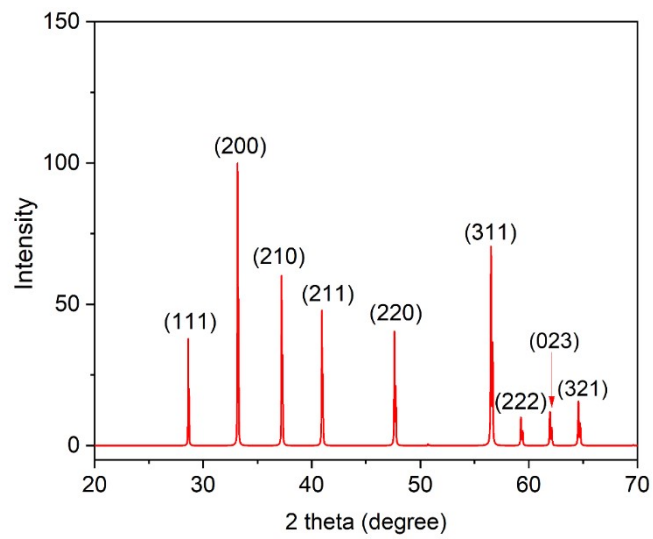


**Figure S1** The grazing-incidence X-ray diffraction of  $\text{FeS}_2$ .<sup>1</sup>

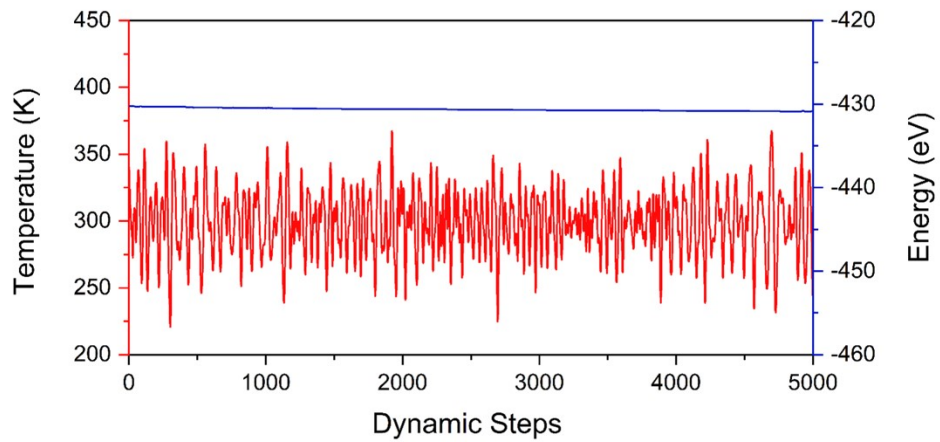


**Figure S2** The temperature and energy fluctuations of  $\text{FeS}_{2-x}(111)\text{-S}_{1V}$  during 10 ps of *ab initio* molecular dynamics (AIMD) simulations.

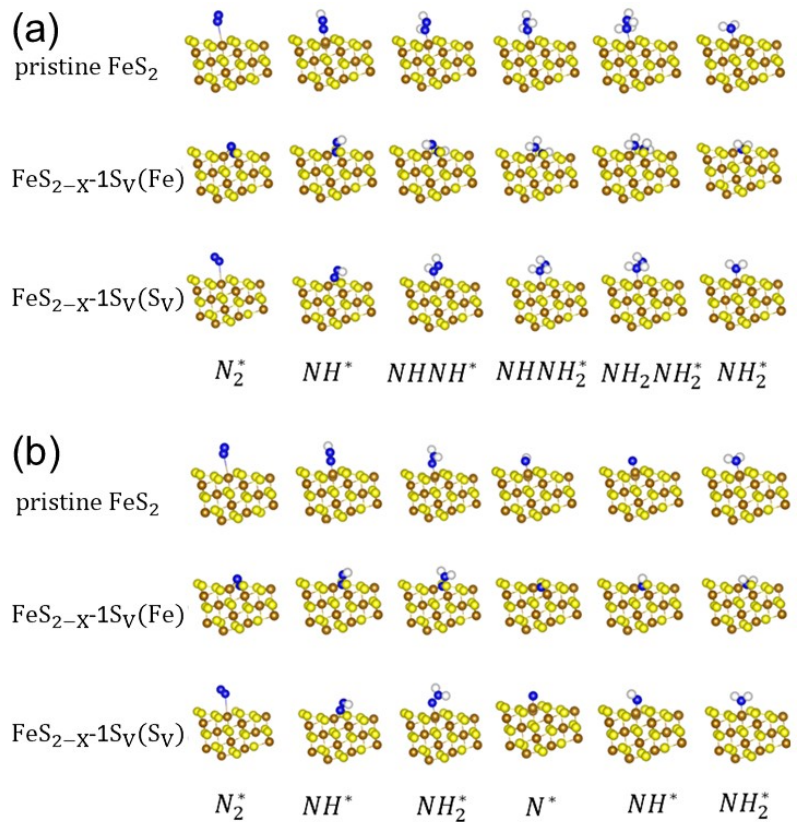


**Figure S3** The optimized configurations of the elementary steps on  $\text{FeS}_2^{(\text{Fe})}(111)$  and  $\text{FeS}_{2-x}(111)\text{-}1\text{S}_\text{V}$  via (a) the alternating and (b) distal pathways.

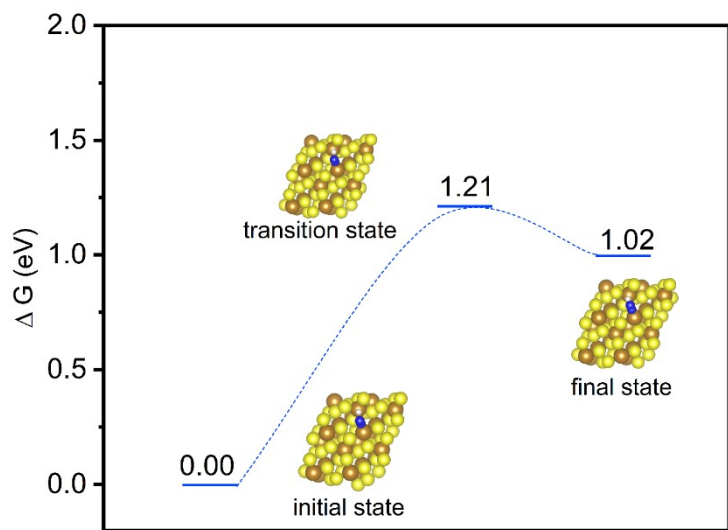


**Figure S4** The transition state of  $N_2^* + H^* \rightarrow NNH^*$  at the Fe site of  $FeS_{2-x}(111)-1S_v$ .

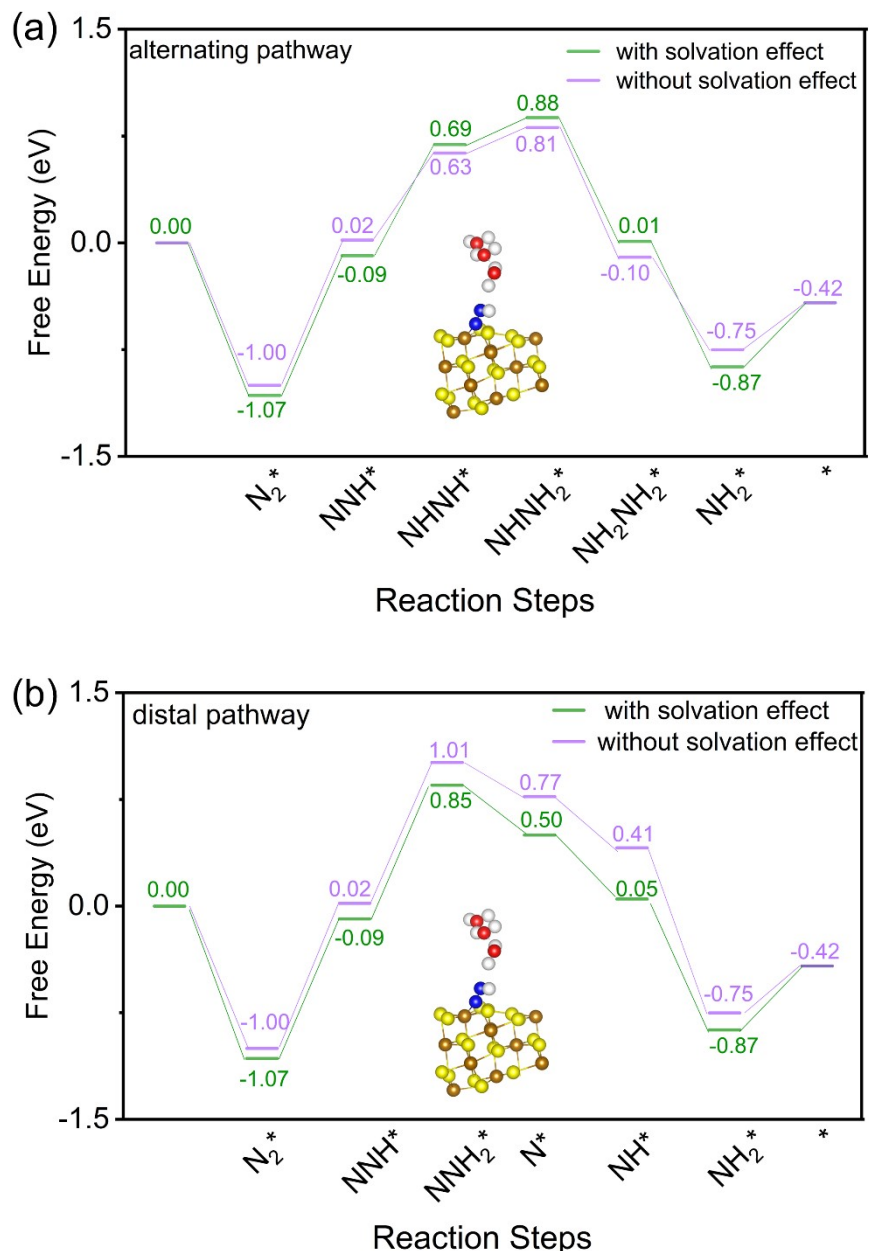


**Figure S5** The energy profiles of ENRR over  $FeS_{2-x}(111)-1S_V$  surfaces at the Fe active site *via* the (a) associative and (b) distal mechanism with and without solvation effects. The optimized  $NNH^*$  with explicit water molecules is inserted. The Fe, S, N, O and H are indicated as brown, yellow, blue, red, and white, respectively.

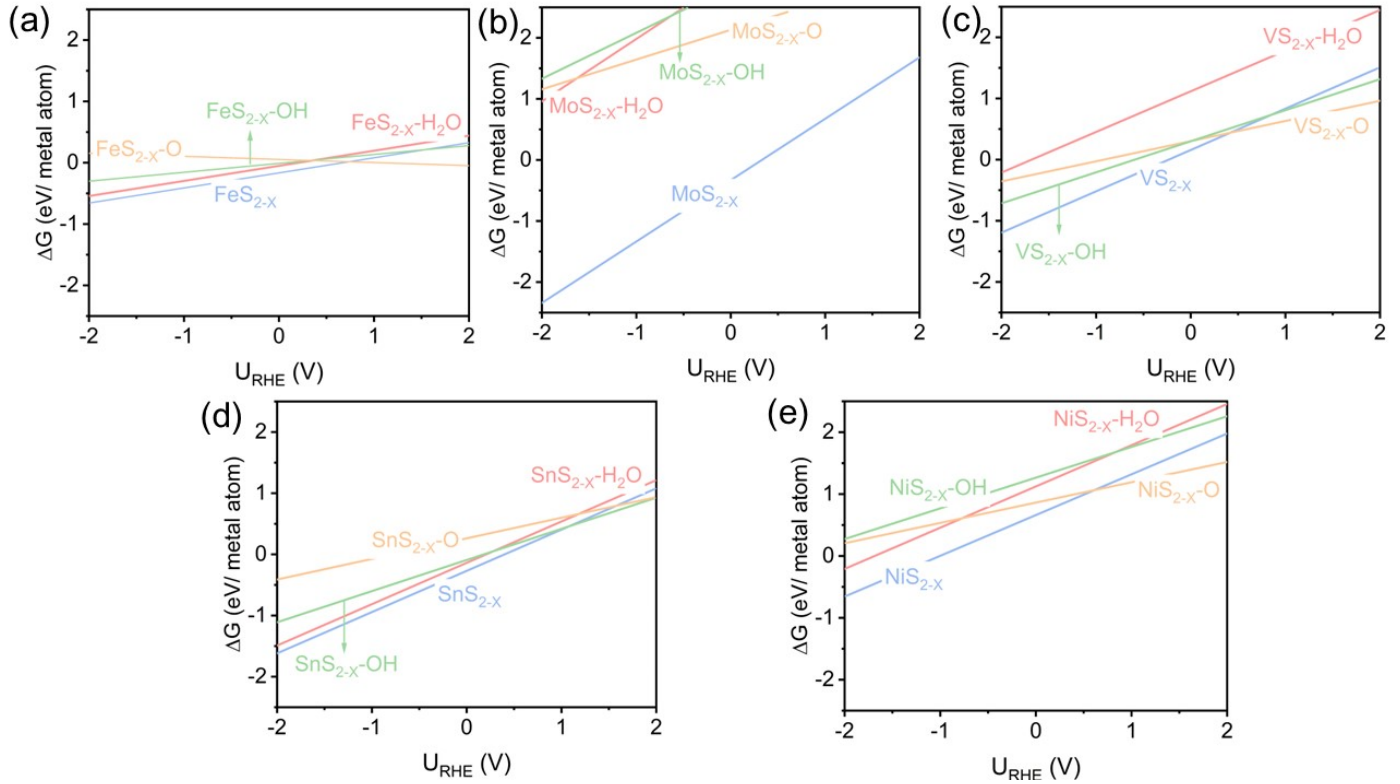


**Figure S6** The surface Pourbaix diagrams of occupied  $\text{H}_2\text{O}^*$ ,  $\text{HO}^*$ , and  $\text{O}^*$  on the  $\text{TMS}_{2-X}$  surfaces.

**Table S1** The highest NH<sub>3</sub> yield, highest Faradic efficiency, and the located potential of FeS<sub>2</sub>-based catalysts via experimental studies.

Catalysts	NH <sub>3</sub> yield	Faradic efficiency (%)	Potential	Refs
			(V vs. RHE)	
FeS <sub>2</sub> /MoS <sub>2</sub> @rGO	41.1 $\mu\text{g h}^{-1} \text{mg}_{\text{cat}}^{-1}$	38.6	-0.2	<sup>2</sup>
FeS <sub>2</sub>	37.2 $\mu\text{g h}^{-1} \text{mg}_{\text{cat}}^{-1}$	11.2	-0.5	<sup>3</sup>
FeS <sub>2</sub> /rGO	27.9 $\mu\text{g h}^{-1} \text{mg}_{\text{cat}}^{-1}$	6.8	-0.3	<sup>4</sup>
Sv-FeS <sub>2</sub>	11.5 $\mu\text{g h}^{-1} \text{mg}_{\text{cat}}^{-1}$	14.6	-0.2	<sup>5</sup>
MoS <sub>2</sub> -FeS <sub>2</sub> /Fe foam	7.1 $\times 10^{-10} \text{ mol s}^{-1} \text{cm}^{-2}$	4.6	-0.5	<sup>6</sup>
Mo-FeS <sub>2</sub>	25.15 $\mu\text{g h}^{-1} \text{mg}_{\text{cat}}^{-1}$	14.4	-0.2	<sup>7</sup>
Sn-FeS <sub>2</sub>	15.8 mg h <sup>-1</sup> cm <sup>-2</sup>	96.7	-0.5	<sup>8</sup>

**Table S2** The calculated surface energies of different FeS<sub>2</sub> facets.

Facet	$E^{\text{unr}}$	$E^{\text{real}}$	a	b	Surface energy (J/m <sup>2</sup> )	
	(eV)	(eV)	(Å)	(Å)	unrelaxed	relaxed
111	-180.26	-181.54	10.93	7.00	1.17	1.03
200	-88.48	-89.27	4.44	5.41	2.40	2.14
210	-174.47	-176.80	10.93	7.00	1.77	1.53
211	-173.57	-176.36	10.93	7.00	1.86	1.57
311	-169.66	-172.44	10.93	7.00	2.27	1.98

**Table S3** The free energies of NNH\* formation, NH<sub>3</sub>\* formation, and NH<sub>3</sub>\* desorption on FeS<sub>2-x</sub>.

Reaction step	Free energy (eV)
$N_2^* + H^* \rightarrow NNH^*$	1.02
$NH_2^* + H^* \rightarrow NH_3^*$	-0.51
$NH_3^* \rightarrow NH_3(g)$	0.84

**Table S4.** The adsorption free energies of N<sub>2</sub> and NH<sub>3</sub> on FeS<sub>2-x</sub> surface.

Species	N <sub>2</sub>	NH <sub>3</sub>
Adsorption free energy (eV)	-1.00	-0.51

**Table S5** The energy barrier of N<sub>2</sub> adsorption and NNH\* formation over FeS<sub>2-x</sub>(111)-1S<sub>V</sub> surfaces at Fe

active site with and without U correction.

	ΔG-DFT (eV)	ΔG-DFT+U (eV)
*+N <sub>2</sub> →NN*	-1.00	-1.06
NN*+H*→NNH*	1.02	1.11

**Table S6** The highest NH<sub>3</sub> yield, highest Faradic efficiency, and the located potential of TMS<sub>2</sub>-based catalysts via experimental studies.

Catalysts	NH <sub>3</sub> yield	Faradic efficiency (%)	Potential (V vs. RHE)	Refs
B-VS <sub>2</sub>	55.7 $\mu\text{g h}^{-1} \text{mg}_{\text{cat}}^{-1}$	16.4	-0.4	<sup>9</sup>
Mo-SnS <sub>2</sub>	41.3 $\mu\text{g h}^{-1} \text{mg}_{\text{cat}}^{-1}$	20.8	-0.4	<sup>10</sup>
V-NiS <sub>2</sub>	47.63 $\mu\text{g h}^{-1} \text{mg}_{\text{cat}}^{-1}$	9.37	-0.35	<sup>11</sup>
Sv-MoS <sub>2</sub>	29.28 $\mu\text{g h}^{-1} \text{mg}_{\text{cat}}^{-1}$	8.34	-0.4	<sup>12</sup>
MoS <sub>2</sub> -PDR	43.4 $\pm$ 3 $\mu\text{g h}^{-1} \text{mg}_{\text{cat}}^{-1}$	16.8 $\pm$ 2	-0.3	<sup>13</sup>
Sv-MoS <sub>2</sub>	23.38 $\mu\text{g h}^{-1} \text{mg}_{\text{cat}}^{-1}$	17.9	-0.35	<sup>14</sup>
Li-S/MoS <sub>2</sub>	43.4 $\mu\text{g h}^{-1} \text{mg}_{\text{cat}}^{-1}$	9.81	-0.2	<sup>15</sup>
MoS <sub>2</sub> /C <sub>3</sub> N <sub>4</sub>	18.5 $\mu\text{g h}^{-1} \text{mg}_{\text{cat}}^{-1}$	17.5	-0.3	<sup>16</sup>
Sn-SnS <sub>2</sub>	23.8 $\mu\text{g h}^{-1} \text{mg}_{\text{cat}}^{-1}$	6.5	-0.7	<sup>17</sup>
MoS <sub>2</sub> -rGO	24.82 $\mu\text{g h}^{-1} \text{mg}_{\text{cat}}^{-1}$	4.56	-0.45	<sup>18</sup>
MoS <sub>2</sub> /CN	36.1 $\mu\text{g h}^{-1} \text{mg}_{\text{cat}}^{-1}$	15.2	-0.5	<sup>19</sup>
Fe-MoS <sub>2</sub>	20.11 $\mu\text{g h}^{-1} \text{mg}_{\text{cat}}^{-1}$	15.72	-0.35	<sup>20</sup>
FL-VS <sub>2</sub>	34.62 $\mu\text{g h}^{-1} \text{mg}_{\text{cat}}^{-1}$	2.09	-0.6	<sup>21</sup>

**Table S7** Formation free energies of the occupying species on FeS<sub>2-x</sub> at -0.2 V<sub>RHE</sub>.

Species	H <sub>2</sub> O*	HO*	O*	N <sub>2</sub> *
Formation free energy (eV)	0.55	0.93	2.09	-1.00

Note: The reason for choosing -0.2 V<sub>RHE</sub> for analysis is because previous works demonstrated that FeS<sub>2</sub> can achieve a high Faradaic efficiency at around -0.2 V<sub>RHE</sub>.<sup>5</sup> The formation free energy ( $\Delta E_{form}$ ) of occupied species on FeS<sub>2-x</sub> surface was calculated *via* Eq. (1):

$$\Delta E_{form} = E_{H_mO^*} + (2 - m) * (0.5 * E_{H2} - U_{SHE} - 2.303 * k * T * pH) - E_{FeS_{2-x}} - E_{H2O} \quad (1)$$

where m is the number of H of occupied species (H<sub>2</sub>O\*, HO\*, and O\*).  $E_{H2O}$ ,  $E_{H2}$ ,  $E_{FeS_{2-x}}$ , and  $E_{H_mO^*}$  are the energies of  $H_2O$  molecule,  $H_2$  molecule, FeS<sub>2-x</sub> surface, and FeS<sub>2-x</sub> surfaces with adsorbed species, respectively.  $U_{SHE}$ ,  $k_B$ , and  $T$  are the potential under the scale of standard hydrogen electrode (SHE), the Boltzmann constant, and temperature, respectively.

## Reference

1. S. Kment, H. Kmentova, A. Sarkar, R. J. Soukup, N. J. Ianno, D. Sekora, J. Olejnicek, P. Ksirova, J. Krysa, Z. Remes and Z. Hubicka, *J. Alloy. Compd.*, 2014, **607**, 169-176.
2. Z. Feng, G. Li, X. Wang, C. J. Gómez-García, J. Xin, H. Ma, H. Pang and K. Gao, *Chem. Eng. J.*, 2022, **445**, 136797.
3. H. Du, C. Yang, W. Pu, L. Zeng and J. Gong, *ACS Sustain. Chem. Eng.*, 2020, **8**, 10572-10580.
4. L. Gao, C. Guo, M. Zhao, H. Yang, X. Ma, C. Liu, X. Liu, X. Sun and Q. Wei, *ACS Appl. Mater. Interfaces*, 2021, **13**, 50027-50036.
5. D. Feng, X. Zhang, Y. Sun and T. Ma, *Nano Mater. Sci.*, 2020, **2**, 132-139.
6. M. Yang, Z. Jin, C. Wang, X. Cao, X. Wang, H. Ma, H. Pang, L. Tan and G. Yang, *ACS Appl. Mater. Interfaces*, 2021, **13**, 55040-55050.
7. H. B. Wang, J. Q. Wang, R. Zhang, C. Q. Cheng, K. W. Qiu, Y. J. Yang, J. Mao, H. Liu, M. Du, C. K. Dong and X. W. Du, *ACS Catal.*, 2020, **10**, 4914-4921.
8. G. Zhang, F. Wang, K. Chen, J. Kang and K. Chu, *Adv. Funct. Mater.*, 2023, 2305372.
9. Q. Li, Y. Guo, Y. Tian, W. Liu and K. Chu, *J. Mater. Chem. A*, 2020, **8**, 16195-16202.
10. K. Chu, J. Wang, Y. P. Liu, Q. Q. Li and Y. L. Guo, *J. Mater. Chem. A*, 2020, **8**, 7117-7124.
11. M. Zhao, C. Guo, L. Gao, X. Kuang, H. Yang, X. Ma, C. Liu, X. Liu, X. Sun and Q. Wei, *Inorg. Chem. Front.*, 2021, **8**, 3266-3272.
12. X. Li, T. Li, Y. Ma, Q. Wei, W. Qiu, H. Guo, X. Shi, P. Zhang, A. M. Asiri, L. Chen, B. Tang and X. Sun, *Adv. Energy Mater.*, 2018, **8**, 1801357.
13. W. Liao, K. Xie, L. Liu, X. Wang, Y. Luo, S. Liang, F. Liu, and L. Jiang, *J. Energy Chem.*, 2021, **62**, 359-366.
14. M. You, S. Yi, X. Hou, Z. Wang, H. Ji, L. Zhang, Y. Wang, Z. Zhang and D. Chen, *J. Colloid. Interface Sci.*, 2021, **599**, 849-856.
15. Y. Liu, M. Han, Q. Xiong, S. Zhang, C. Zhao, W. Gong, G. Wang, H. Zhang and H. Zhao, *Adv. Energy Mater.*, 2019, **9**, 1803935.
16. K. Chu, Y. P. Liu, Y. B. Li, Y. L. Guo and Y. Tian, *T., ACS Appl. Mater. Interfaces*, 2020, **12**, 7081-7090.
17. P. Li, W. Fu, P. Zhuang, Y. Cao, C. Tang, A. B. Watson, P. Dong, J. Shen and M. Ye, *Small*, 2019, **15**, e1902535.
18. X. Li, X. Ren, X. Liu, J. Zhao, X. Sun, Y. Zhang, X. Kuang, T. Yan, Q. Wei and D. Wu, *J. Mater. Chem. A*, 2019, **7**, 2524-2528.

19. X. W. Lv, X. L. Liu, Y. J. Suo, Y. P. Liu and Z. Y. Yuan, *ACS Nano*, 2021, **15**, 12109-12118.
20. L. Niu, D. Wang, K. Xu, W. Hao, L. An, Z. Kang and Z. Sun, *Nano Res.*, 2021, **14**, 4093-4099.
21. L. Zhao, R. Zhao, Y. Zhou, X. Wang, X. Chi, Y. Xiong, C. Li, Y. Zhao, H. Wang, Z. Yang and Y. M. Yan, *J. Mater. Chem. A*, 2021, **9**, 24985-24992.